Analytical Model for the Open Circuit Field due to Different Magnetization Patterns of the rotor in the Slotless Machines

Nisarg Dave, David Gerada, Gaurang Vakil, He Zhang, Jing Li, Chris Gerada

***Abstract* – From the existing literature, the open circuit field due to different magnetisations of the rotor magnets is known. This includes field due to parallel, radial and Halbach magnetisation. This paper presents the generalised analytical model to represent the open circuit fields due to these three magnetisations for a slotless machine. With the armature reaction field, the vector summation of the open circuit field and armature reaction field in the air gap gives the airgap flux density field, which is crucial for evaluating performance parameters and machine behaviour.**

***Index Terms*— analytical modelling, field due to magnets, open circuit field, slotless machine, sub domain model.**

I. Nomenclature

A_w	Magnetic vector potential in the winding region
r	Radius for measurement
θ	Angle for measurement with respect to the center of the magnet pole
A_m	Magnetic vector potential in the magnet region
μ_0	Permeability of the free space
μ_r	Relative permeability of the magnets
$\vec{M}$	Magnetisation vector
n	Harmonic order
p	Number of pole-pair
M_{radial}	Radial component of magnetisation vector
$M_{tangential}$	Tangential component of magnetisation vector
$B_{w\theta}$	Tangential component of flux density in winding region
$B_{m\theta}$	Tangential component of flux density in magnet region
B_{wr}	Radial component of flux density in winding region
B_{mr}	Radial component of flux density in magnet region
ω	Angular frequency
t	Time in seconds
α_p	Pole span
α_c	Coil span
B_r	Remanence flux density of the magnets
$\Psi_\emptyset$	Flux linkage in-phase ($\emptyset$ = a, b or c)
L	Stack length
N_c	Number of turns per coil
C	Total number of coils
a	Number of parallel paths
k_{wn}	The winding factor of a slotless machine
k_{cpn}	Conductor pitch factor
k_{cdn}	Conductor distribution factor
k_{dn}	Winding distribution factor
F_n	Force constant of slotless machine
$e_\emptyset$	Induced back emf of phase ($\emptyset$ = a, b, or c)

II. Introduction

THE open-circuit magnetic field calculation is crucial to analysing the performance of slotless permanent magnet machines. The flux linkages in the coil, back-EMF and iron losses of the concentrated windings machine can be derived by accurately obtaining the open-circuit magnetic field. Furthermore, electromagnetic torque and unbalanced magnetic pull can be calculated from the vector summation of the open-circuit field and the armature reaction field.

This study focuses on slotless machines with different magnetisation patterns and inner and outer rotor structures. The analytical open-circuit magnetic field calculation has been presented in [1]–[4]. The open-circuit magnetic field calculation has been presented for different magnetisation patterns in various machine regions, i.e., winding, PM, and airgap regions. The [4] describes the open-circuit field due to parallel and radial magnetisation patterns for inner and outer rotor structures. It also talks about the effect of slotting and considering the infinite permeability of iron. [1]–[3] talks about different Halbach magnetisation patterns. [1] talks about magnetisation due to the Halbach array for inner rotor and outer rotor structure. This paper has also considered the equation for the different relative permeability of the magnet.

This work is supported by Ministry of Science & Technology under National Key R&D Program of China, under Grant 2021YFE0108600.

N. Dave, D. Gerada and C. Gerada are with PEMC group, University of Nottingham, UK campus and University of Nottingham Ningbo China (e-mail: Nisarg.Dave@nottingham.edu.cn).

G. Vakil is with PEMC group, University of Nottingham, UK campus. H. Zhang and J. Li are with PEMC group, University of Nottingham Ningbo China.

Moreover, the study extends to the inner and outer rotor structures by calculating the magnetic field in different machine regions. [2] talks about open-circuit field and calculation due to 2-segment Halbach array and internal rotor topology. This study is performed for the unity value of the relative permeability of the permanent magnets. The analysis presented in paper [3] discusses bar-shifting magnetisation patterns for inner rotor structures. The work is also extended for the slotting effect in the slotted motor, and results are derived. The paper [5] also gives a good idea for different magnetisation patterns for slotless machines and derives back emf and torque calculations for the distributed winding slotless machine.

This paper discusses the analytical calculation of open-circuit magnetic field for three magnetisation patterns, i.e., parallel, radial and Halbach. Also, the study is extended to the inner rotor and outer rotor structure. In addition, the flux linkages and back emf calculations have been performed for winding patterns. Finally, the results of this study are validated with commercially available FEA software with high accuracy.

III. FIELD DUE TO MAGNETS

In order to provide accurate magnetic field analysis for internal and external rotors for three different magnetisation patterns, i.e. Uniform, Radial as shown in Fig. 1 and Halbach as shown in Fig. 2, the sub-domain modelling approach is used as mentioned in [1]–[4]. The equations, responsible for this field and validation of these equation to the finite element analysis is demonstrated in following sections.

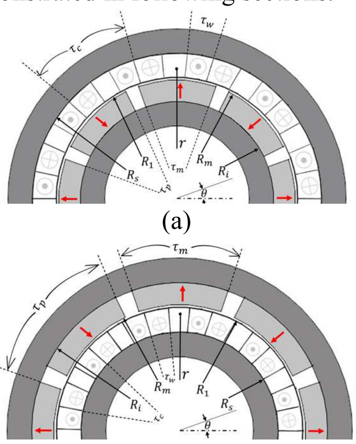

Fig. 1 Internal (a) and external (b) rotor structure with uniform/radial magnets and nomenclature

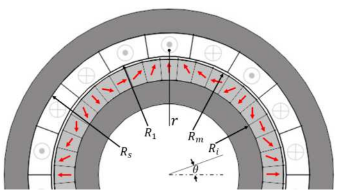

(a)

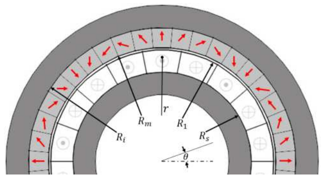

(b)

Fig. 2 Internal and External Rotor structure and nomenclature for Halbach magnets

The machine under study in this paper has following dimensions R_i = 40mm, R_1 = 50mm, R_s = 60mm, R_m = 49mm for inner rotor and R_i = 60mm, R_1 = 50mm, R_s = 40mm, R_m = 51mm for outer rotor. For both topologies, Length = 25mm and number of turns = 35.

The general solution for the magnetic field in the airspace is given by the general solution of Laplacian/quasi-Poissonian equations and specified boundary conditions [8].

In the winding and airgap region,

$$\frac{\partial^2 A_w}{\partial r^2} + \frac{1}{r}\frac{\partial A_w}{\partial r} + \frac{1}{r^2}\frac{\partial^2 A_w}{\partial \theta^2} = 0 \tag{1}$$

In the magnet region,

$$\frac{\partial^2 A_m}{\partial r^2} + \frac{1}{r}\frac{\partial A_m}{\partial r} + \frac{1}{r^2}\frac{\partial^2 A_m}{\partial \theta^2} = \frac{1}{\mu_r}\nabla \cdot \vec{M} \tag{2}$$

Where,

$$\nabla \cdot \vec{M} = \sum_{n=1,3,5\ldots}^{\infty} \frac{1}{r} M_n \cos(np\theta) \tag{3}$$

And,

$$M_n = M_{radial} + npM_{tangential} \tag{4}$$

The boundary conditions for internal and external rotor can be defined as,

$$\begin{aligned} B_{w\theta}(r,\theta)\big|_{r=R_s} &= 0 \\ B_{m\theta}(r,\theta)\big|_{r=R_i} &= 0 \\ B_{wr}(r,\theta)\big|_{r=R_m} &= B_{mr}(r,\theta)\big|_{r=R_m} \\ B_{w\theta}(r,\theta)\big|_{r=R_m} &= B_{m\theta}(r,\theta)\big|_{r=R_m} \end{aligned} \tag{5}$$

Where, R_s, R_i *and* R_m are as defined in Fig.1(a) and Fig.2(a) for the inner rotor and Fig.1(b) and Fig.2(b) for the outer rotor. The following equations give the general solution for any magnetisation for np≠1.

$$A_w(r,\theta) = \sum_{n=1,3,5\ldots}^{\infty} (a_w r^{np} + b_w r^{-np}) \sin(np\theta - n\omega t) \tag{6}$$

$$A_m(r,\theta) = \sum_{n=1,3,5\ldots}^{\infty} \left((a_m r^{np} + b_m r^{-np}) + \frac{M_n}{\mu_r(1-(np)^2)} \right) \sin(np\theta - n\omega t) \quad (7)$$

for $np = 1$ following equation is used,

$$A_m(r,\theta) = (a_m r^{np} + b_m r^{-np}) \cos(\theta - \omega t) + \frac{1}{2}\frac{M_1}{\mu_r} r \ln(r) \cos\theta \quad (8)$$

The winding current is kept zero for calculating the field only due to magnets. So, the winding region is considered airspace as the machine is slotless. The field in the winding region due to magnets is given by vector summation of radial and tangential flux density,

$$B_w = B_{wr}\hat{r} + B_{w\theta}\hat{\theta} = \frac{1}{r}\frac{\partial A_w}{\partial \theta}\hat{r} - \frac{\partial A_w}{\partial r}\hat{\theta} \quad (9)$$

The solution of the above equation gives,

$$B_{wr} = \sum_{n=1,3,5\ldots}^{\infty} (np) \cdot \left(a_w r^{(np)-1} + b_w r^{(-np)-1}\right) \cos(np\theta - n\omega t) \quad (10)$$

$$B_{w\theta} = \sum_{n=1,3,5\ldots}^{\infty} (-np) \cdot \left(a_w r^{(np)-1} - b_w r^{(-np)-1}\right) \sin(np\theta - n\omega t) \quad (11)$$

Where, a_w and b_w are the co-efficient which varies in each case, for Halbach magnets $n = 1$.

A. Uniform and Radial magnets:

The coefficients for inner rotor uniform and radial magnets can be defined for $np \neq 1$ as follow,

$$a_w = X_1 X_2 R_s^{-2np} \quad (12)$$

$$b_w = X_1 X_2 \quad (13)$$

And,

$$X_1 = \left\{ \frac{(A_{3n}-1) + 2\left(\frac{R_i}{R_m}\right)^{np+1} - (A_{3n}+1)\left(\frac{R_i}{R_m}\right)^{2np}}{\frac{\mu_r+1}{\mu_r}\left[1-\left(\frac{R_i}{R_s}\right)^{2np}\right] - \frac{\mu_r-1}{\mu_r}\left[\left(\frac{R_m}{R_s}\right)^{2np} - \left(\frac{R_i}{R_m}\right)^{2np}\right]} \right\} \quad (14)$$

$$X_2 = \frac{\mu_0 M_n}{\mu_r}\frac{1}{(np)^2-1} R_m^{np+1} \quad (15)$$

For inner rotor radial and uniform magnets where $np = 1$, the coefficient becomes as follows,

$$a_w = X_1 X_2 \quad (16)$$

$$b_w = X_1 X_2 R_s^2 \quad (17)$$

$$X_1 = \left\{ \frac{A_{3n}\left(\frac{R_m}{R_s}\right)^2 - A_{3n}\left(\frac{R_i}{R_s}\right)^2 + \left(\frac{R_i}{R_s}\right)^2 \ln\left(\frac{R_m}{R_i}\right)^2}{\frac{\mu_r+1}{\mu_r}\left[1-\left(\frac{R_i}{R_s}\right)^2\right] - \frac{\mu_r-1}{\mu_r}\left[\left(\frac{R_m}{R_s}\right)^2 - \left(\frac{R_i}{R_m}\right)^2\right]} \right\} \quad (18)$$

$$X_2 = \frac{\mu_0 M_n}{2\mu_r} \quad (19)$$

For outer rotor structure, the coefficients are defined as follow,

$$a_w = \begin{cases} -X_1 X_2 R_s^{-2np} & for\ np \neq 1 \\ -X_1 X_2 & for\ np = 1 \end{cases} \quad (20)$$

$$b_w = \begin{cases} -X_1 X_2 & for\ np \neq 1 \\ -X_1 X_2 R_s^2 & for\ np = 1 \end{cases} \quad (21)$$

Where, X_1 and X_2 are as defined as equations (14), (15) and (18), (19) for $np \neq 1$ and $np = 1$, respectively.

For Uniform magnets,

$$A_{1n} = \frac{\sin\left[(np+1)\alpha_p \frac{\pi}{2p}\right]}{(np+1)\alpha_p \frac{\pi}{2p}} \quad (22)$$

$$A_{2n} = 1 \text{ (for np = 1)} \quad (23)$$

$$A_{2n} = \frac{\sin\left[(np-1)\alpha_p \frac{\pi}{2p}\right]}{(np-1)\alpha_p \frac{\pi}{2p}} \text{ (for np} \neq 1) \quad (24)$$

$$M_{radial} = \frac{B_r}{\mu_0}\alpha_p (A_{1n} + A_{2n}) \quad (25)$$

$$M_{tangential} = \frac{B_r}{\mu_0}\alpha_p (A_{1n} - A_{2n}) \quad (26)$$

$$A_{3n} = 2\frac{M_{radial}}{M_n} - 1 \text{ (for np = 1)} \quad (27)$$

$$A_{3n} = \left(np - \frac{1}{np}\right)\frac{M_{radial}}{M_n} + \frac{1}{np} \text{ (for np} \neq 1) \quad (28)$$

Here,

$$\alpha_p = \frac{\tau_m}{\tau_p} \quad (29)$$

M_n is as defined in equation (4).

And for radially magnetised magnets following parameter changes.

$$M_{radial} = 2\frac{B_r}{\mu_0}\alpha_p \frac{\sin\frac{n\pi\alpha_p}{2}}{\frac{n\pi\alpha_p}{2}} \quad (30)$$

$$M_{tangential} = 0 \quad (31)$$

$$A_{3n} = np \tag{32}$$

B. Halbach Magnets:

The coefficients for the Halbach magnetised inner rotor (external field) where n = 1 can be described as follow,

$$a_w = \frac{X_1}{X_2} R_s^{-2p} \tag{33}$$

$$b_w = \frac{X_1}{X_2} \tag{34}$$

$$X_1 = 4B_r \frac{1}{p+1}\left\{1 - \left(\frac{R_i}{R_m}\right)^{p+1}\right\} R_m^{p+1} \tag{35}$$

$$X_2 = 2\left[\left(\frac{R_i}{R_m}\right)^{2p}\left\{(1-\mu_r) + (1+\mu_r)\left(\frac{R_m}{R_s}\right)^{2p}\right\} - \left\{(1+\mu_r) + (1-\mu_r)\left(\frac{R_m}{R_s}\right)^{2p}\right\}\right] \tag{36}$$

The coefficients for the Halbach magnetised outer rotor (internal field) where n = 1 can be described as follow,

$$a_w = \frac{X_1}{X_2} \tag{37}$$

$$b_w = \frac{X_1}{X_2} R_s^{2p} \tag{38}$$

$$X_1 = 4B_r \frac{1}{1-p}\left\{1 - \left(\frac{R_m}{R_i}\right)^{p-1}\right\} R_m^{(-p)+1} \tag{39}$$

$$X_2 = 2\left[(1-\mu_r)\left(\frac{R_m}{R_i}\right)^{2p} + (1+\mu_r)\left(\frac{R_s}{R_i}\right)^{2p} - \left\{(1+\mu_r) + (1-\mu_r)\left(\frac{R_s}{R_m}\right)^{2p}\right\}\right] \tag{40}$$

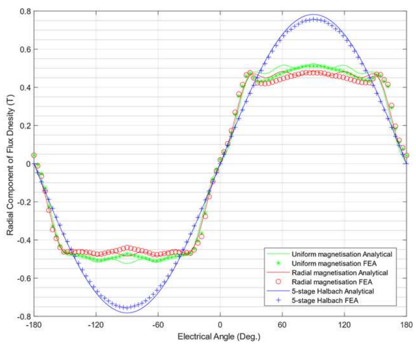

Fig. 3 Radial component of magnetic field density due to PM only at r = $(R_1 + R_m)/2$ and t=0 for internal rotor motor

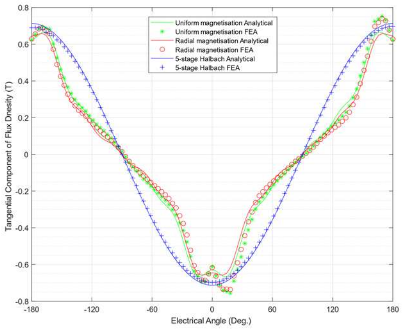

Fig. 4 Tangential component of magnetic field density due to PM only at r = $(R_1 + R_m)/2$ and t=0 for internal rotor motor

TABLE 1
VALIDATION FOR FEA & ANALYTICALLY CALCULATED RADIAL MAGNETIC FIELD DUE TO MAGNETS

Cases	RMS Analytical $\boldsymbol{B_r}$ (T)	RMS FEA $\boldsymbol{B_r}$ (T)	% Variation
12C-16P, IR, Uniform magnets, $\boldsymbol{\alpha_p}$ = 0.85	0.4354	0.4301	-1.2328%
12C-16P, IR, Radial magnets, $\boldsymbol{\alpha_p}$ = 0.85	0.4162	0.4126	-0.8725%
12C-16P, IR, Halbach magnets, $\boldsymbol{\alpha_p}$ = 1	0.5505	0.5470	-2.5081%

TABLE 2
VALIDATION FOR FEA & ANALYTICALLY CALCULATED TANGENTIAL MAGNETIC FIELD DUE TO MAGNETS

Cases	RMS Analytical $\boldsymbol{B_t}$ (T)	RMS FEA $\boldsymbol{B_t}$ (T)	% Variation
12C-16P, IR, Uniform magnets, $\boldsymbol{\alpha_p}$ = 0.85	0.4036	0.4207	4.0748%
12C-16P, IR, Radial magnets, $\boldsymbol{\alpha_p}$ = 0.85	0.3871	0.4040	4.1795%
12C-16P, IR, Halbach magnets, $\boldsymbol{\alpha_p}$ = 1	0.5070	0.4949	2.4450%

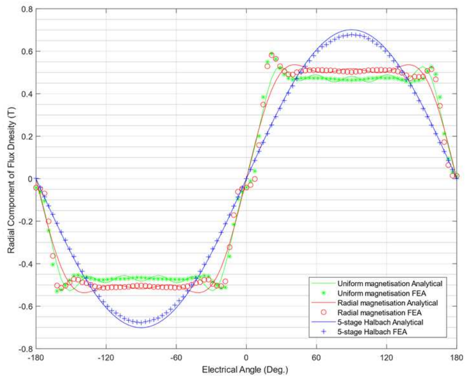

Fig. 5 Radial component of magnetic field density due to PM only at r = $(R_1 + R_m)/2$ and t=0 for outer rotor motor

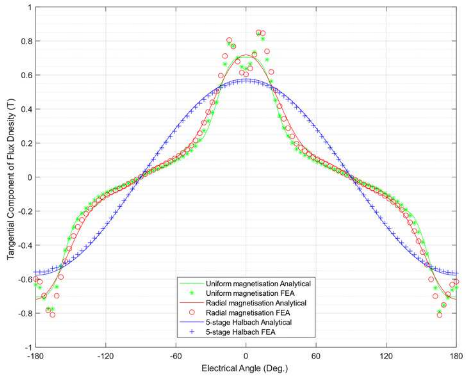

Fig. 6 Tangential component of magnetic field density due to PM only at r $= (R_1 + R_m)/2$ and t=0 for outer rotor motor

TABLE 3
VALIDATION FOR FEA & ANALYTICALLY CALCULATED RADIAL MAGNETIC FIELD DUE TO MAGNETS

Cases	Average Analytical B_r (T)	Average FEA B_r (T)	% Variation
15C-10P, OR, Uniform magnets, $\alpha_p = 0.85$	0.4389	0.4407	0.4232%
15C-10P, OR, Radial magnets, $\alpha_p = 0.85$	0.4595	0.4613	0.3862%
15C-10P, OR, Halbach magnets, $\alpha_p = 1$	0.4935	0.4795	-2.9197%

TABLE 4
VALIDATION FOR FEA & ANALYTICALLY CALCULATED TANGENTIAL MAGNETIC FIELD DUE TO MAGNETS

Cases	Average Analytical B_t (T)	Average FEA B_t (T)	% Variation
15C-10P, OR, Uniform magnets, $\alpha_p = 0.85$	0.3756	0.3927	4.3356%
15C-10P, OR, Radial magnets, $\alpha_p = 0.85$	0.3905	0.4086	4.4274%
15C-10P, OR, Halbach magnets, $\alpha_p = 1$	0.4101	0.4003	2.4482%

IV. FLUX LINKAGE AND BACK EMF CALCULATION

The slotless machine's flux linkage and back emf calculations have been discussed in [6] and [7]. To calculate flux linkage in the phase, first, the flux linkage in the coil should be determined. The field due to magnet and winding arrangement are two critical factors to determine the flux linkage and back emf. The equation of field due to the magnets is already mentioned in Section II and can be re-written as,

$$B_{wr} = \sum_{n=1,3,5\ldots}^{\infty} B_{rn}\cos(np\theta - n\omega t) \tag{41}$$

$$B_{w\theta} = \sum_{n=1,3,5\ldots}^{\infty} B_{\theta n}\sin(np\theta - n\omega t) \tag{42}$$

Where, B_{rn} and $B_{\theta n}$ are as mentioned in equation (10) and (11).

$$\alpha_c = \frac{2\tau_w}{\tau_c} \tag{43}$$

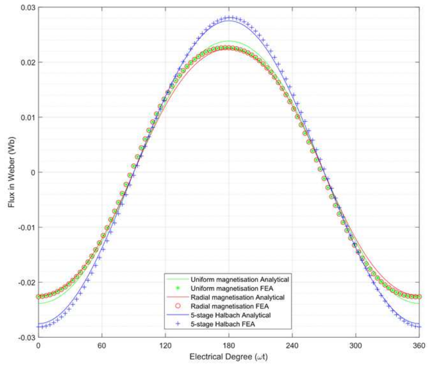

Fig. 7 Flux linkage for 15-Coils 10-Pole inner rotor slotless machine with α_c= 0.75 for uniform, radial and Halbach magnetization

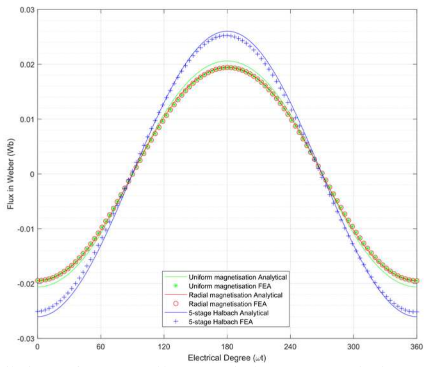

Fig. 8 Flux linkage for 18-Coils 14-Pole inner rotor slotless machine with α_c= 0.6 for uniform, radial and Halbach magnetization

TABLE 5
VALIDATION FOR FEA & ANALYTICALLY CALCULATED FLUX LINKAGE IN PHASE-A

Cases	RMS Analytical (Wb)	RMS FEA (Wb)	% Variation
15C-10P, IR, Uniform magnets, $\alpha_p = 0.85$, $\alpha_c = 0.75$	0.0173	0.0168	-2.7101%
15C-10P, IR, Radial magnets, $\alpha_p = 0.85$, $\alpha_c = 0.75$	0.0163	0.0168	2.7751%
15C-10P, IR, Halbach magnets, $\alpha_p = 1$, $\alpha_c = 0.75$	0.0196	0.0200	2.0325%
18C-14P, IR, Uniform magnets, $\alpha_p = 0.85$, $\alpha_c = 0.6$	0.0149	0.0140	-6.7090%
18C-14P, IR, Radial magnets, $\alpha_p = 0.85$, $\alpha_c = 0.6$	0.0141	0.0140	-1.0361%
18C-14P, IR, Halbach magnets, $\alpha_p = 1$, $\alpha_c = 0.6$	0.0185	0.0179	-3.5114%

As mentioned in paper [6], the equation for the flux linkage in each phase can be written as,

$$\Psi_a = \sum_{n=1,3,5\ldots}^{\infty} \frac{2LN_cC}{3anp} k_{wn}F_n\cos(n\omega t) \tag{44}$$

$$\Psi_b = \sum_{n=1,3,5\ldots}^{\infty} \frac{2LN_cC}{3anp} k_{wn} F_n \cos\left(n\omega t - \frac{2\pi}{3}\right) \qquad (45)$$

$$\Psi_c = \sum_{n=1,3,5\ldots}^{\infty} \frac{2LN_cC}{3anp} k_{wn} F_n \cos\left(n\omega t - \frac{4\pi}{3}\right) \qquad (46)$$

Where,
k_{wn} is the winding factor defined as,

$$k_{wn} = k_{cpn} k_{cdn} k_{dn} \qquad (47)$$

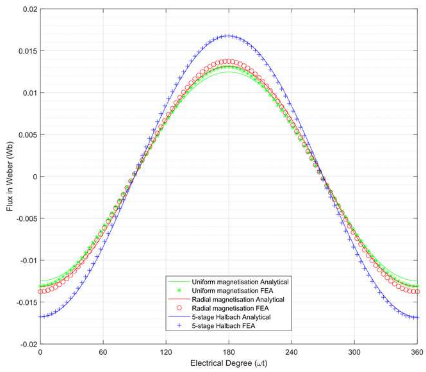

Fig. 9 Flux linkage for 12-Coils 16-Pole outer rotor slotless machine with α_c= 0.6 for uniform, radial and Halbach magnetization

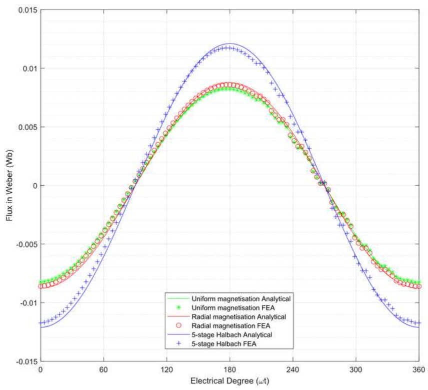

Fig. 10 Flux linkage for 18-Coils 22-Pole outer rotor slotless machine with α_c= 0.9 for uniform, radial and Halbach magnetisation

TABLE 6
VALIDATION FOR FEA & ANALYTICALLY CALCULATED FLUX LINKAGE IN PHASE-A

Cases	RMS Analytical (Wb)	RMS FEA (Wb)	% Variation
12C-16P, OR, Uniform magnets, α_p = 0.85, α_c = 0.6	0.0090	0.0092	2.3672%
12C-16P, OR, Radial magnets, α_p = 0.85, α_c = 0.6	0.0095	0.0097	2.1353%
12C-16P, OR, Halbach magnets, α_p = 1, α_c = 0.6	0.0119	0.0119	0.0861%
18C-22P, OR, Uniform magnets, α_p = 0.85, α_c = 0.9	0.0060	0.0058	-2.5212%
18C-22P, OR, Radial magnets, α_p = 0.85, α_c = 0.9	0.0063	0.0061	-2.7769%
18C-22P, OR, Halbach magnets, α_p = 1, α_c = 0.9	0.0086	0.0083	-3.5480%

And k_{cpn}, k_{cdn} and k_{dn} are as defined in [6].

$$F_n = \frac{1}{R_s - R_1} \int_{R_1}^{R_s} r B_{rn}(r) dr \qquad (48)$$

The back emf can be represented by the derivative of flux linkage in the coil regarding time. The equation of the back emf can be written as follow.

$$e_\emptyset(t) = \frac{d\Psi_\emptyset(t)}{dt} \qquad (49)$$

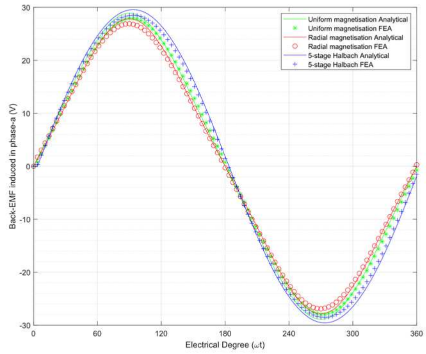

Fig. 11 Back emf for 9-Coils 8-Pole inner rotor slotless machine with α_c= 0.9 for uniform, radial and Halbach magnetisation

The validation of these equations against the FEA tool against various cases of inner rotor, outer rotor, different magnetisation patterns and different concentrated winding cases are presented in the graphs.

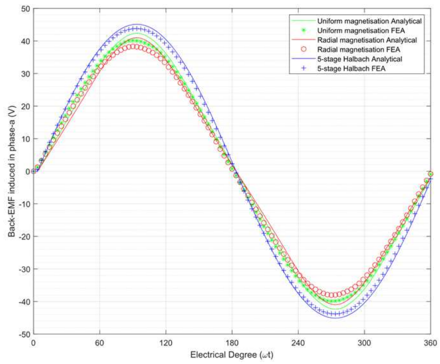

Fig. 12 Back emf for 12-Coils 10-Pole inner rotor slotless machine with α_c= 0.6 for uniform, radial and Halbach magnetization

TABLE 7
VALIDATION FOR FEA & ANALYTICALLY CALCULATED BACK EMF IN PHASE-A

Cases	RMS Analytical (V)	RMS FEA (V)	% Variation
9C-8P, IR, Uniform magnets, α_p = 0.85, α_c = 0.9	19.4575	18.9914	-2.4543%
9C-8P, IR, Radial magnets, α_p = 0.85, α_c = 0.9	18.4876	18.0746	-2.2852%
9C-8P, IR, Halbach magnets, α_p = 1, α_c = 0.9	20.8129	20.0694	-3.7047%
12C-10P, IR, Uniform magnets, α_p = 0.85, α_c = 0.6	28.0914	27.5247	-2.0588%
12C-10P, IR, Radial magnets, α_p = 0.85, α_c = 0.6	26.6245	26.1170	-1.9430%

12C-10P, IR, Halbach magnets, α_p = 1, α_c = 0.6	31.7505	30.8455	-2.9340%

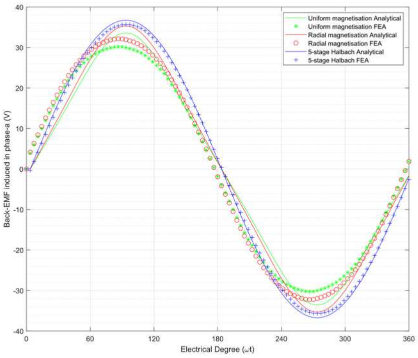

Fig. 13 Back emf for 9-Coils 10-Pole outer rotor slotless machine with α_c= 0.6 for uniform, radial and Halbach magnetization

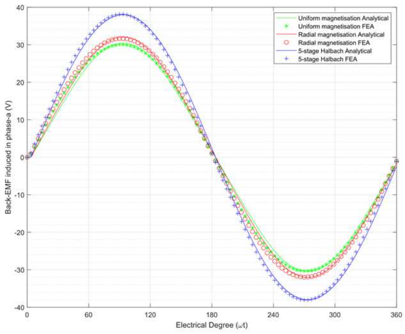

Fig. 14 Back emf for 12-Coils 14-Pole outer rotor slotless machine with α_c= 0.85 for uniform, radial and Halbach magnetization

TABLE 8
VALIDATION FOR FEA & ANALYTICALLY CALCULATED BACK EMF IN PHASE-A

Cases	RMS Analytical (V)	RMS FEA (V)	% Variation
9C-10P, OR, Uniform magnets, α_p = 0.85, α_c = 0.6	21.9406	21.8918	-0.2228%
9C-10P, OR, Radial magnets, α_p = 0.85, α_c = 0.6	23.3044	23.2326	-0.3088%
9C-10P, OR, Halbach magnets, α_p = 1, α_c = 0.6	25.8462	25.1314	-2.8444%
12C-14P, OR, Uniform magnets, α_p = 0.85, α_c = 0.85	20.8687	21.3970	2.4690%
12C-14P, OR, Radial magnets, α_p = 0.85, α_c = 0.85	22.0343	22.5526	2.2985%
12C-14P, OR, Halbach magnets, α_p = 1, α_c = 0.85	26.7460	26.8538	0.4012%

V. CONCLUSION

The paper presents a robust generalised analytical model to predict the airgap flux density in the air gap and the winding region at no-load conditions. The model can be used for parallel, radial or Halbach magnetisation to compute the no-load analysis of slotless machines with a concentrated winding. Furthermore, the generalised sub-domain analytical model can drastically reduce the computation time to finite element analysis method for no-load calculations. Finally, only the no-load calculation method has been described in this paper due to space restriction. With the limited extension, the approach can be adapted to cover the armature reaction field due to the sinusoidal current in the concentrated wound slotless machine. With vector summation of these two waveforms, the airgap flux density at the on-load condition can be predicted analytically. Such extension and relevant performance study with experimental validation will be presented in future publications.

VI. REFERENCES

[1] Z. P. Xia, Z. Q. Zhu, and D. Howe, "Analytical magnetic field analysis of Halbach magnetised permanent-magnet machines," IEEE Trans. Magn., vol. 40, no. 4 I, pp. 1864–1872, 2004.
[2] M. Markovic and Y. Perriard, "Optimisation design of a segmented Halbach permanent-Magnet motor using an analytical model," IEEE Trans. Magn., vol. 45, no. 7, pp. 2955–2960, 2009.
[3] K. Boughrara, B. L. Chikouche, R. Ibtiouen, D. Zarko, and O. Touhami, "Analytical model of slotted airgap surface-mounted permanent-magnet synchronous motor with magnet bars magnetised in the shifting direction," IEEE Trans. Magn., vol. 45, no. 2, pp. 747–758, 2009.
[4] Zhu, Z. Q., David Howe, C. C. Chan, "Improved Analytical Model for Predicting the Magnetic Field Distribution in Brushless Permanent-Magnet Machines," IEEE Trans. Magn., vol. 38, no. 1, pp. 229–238, 2002.
[5] A. Rahideh and T. Korakianitis, "Analytical magnetic field distribution of slotless brushless PM motors. Part 2: Open-circuit field and torque calculations," IET Electr. Power Appl., vol. 6, no. 9, pp. 639–651, 2012.
[6] S. G. Min, S. Member, B. Sarlioglu, and S. Member, "Advantages and Characteristic Analysis of Slotless Rotary PM Machines in Comparison with Using Statistical Technique," vol. 4, no. 2, pp. 517–524, 2018.
[7] Z. Song, C. Liu, and H. Zhao, "Comparative Analysis of Slotless and Coreless Permanent Magnet Synchronous Machines for Electric Aircraft Propulsion," 2019 22nd Int. Conf. Electr. Mach. Syst. ICEMS 2019, 2019.
[8] A. Hughes and T. J. E. Miller, "Analysis of fields and inductances in air-cored and iron-cored synchronous machines," Proc. Inst. Elect. Eng., vol. 124, no. 2, pp. 121–126, 1977

Nisarg Dave joined the Power Electronics, Machines and Control (PEMC) Group at the University of Nottingham in 2018, where he is currently pursuing his PhD.

David Gerada (Senior Member, IEEE) received the Ph.D. degree in high-speed electrical machines from the University of Nottingham, Nottingham, U.K., in 2012. He is currently a Principal Research Fellow in electrical machines with the same institute. Dr. Gerada is a Chartered Engineer in the U.K. and a member of the Institution of Engineering and Technology.

Gaurang Vakil received the Ph.D. degree from the Power Electronics, Machines and Drives Group, IIT Delhi, New Delhi, India, in 2016. He subsequently joined the Power Electronics, Machines and Controls Group, University of Nottingham, Nottingham, U.K. He is an Associate Professor from 2022 at the same institution.

Prof. He Zhang (M'14-SM'18) obtained the MSc. and Ph.D. degree in electrical machines from The University of Nottingham, UK, in 2004 and 2009 respectively. Currently he is the Director of Nottingham Electrification Centre within the Power electronics, Machines and Control research group in University of Nottingham.

Jing Li (M'15) received the Ph.D. degree in electrical engineering from the University of Nottingham, Nottingham, U.K, in 2010. She is currently an Associate Professor with electrical and electronics engineering department, University of Nottingham Ningbo China.

Chris Gerada (Senior Member, IEEE) received the Ph.D. degree in numerical modeling of electrical machines from the University of Nottingham, Nottingham, U.K., in 2005. He is currently an Associate Pro-Vice-Chancellor for industrial strategy and impact and a Professor of electrical machines with the University of Nottingham. Dr. Gerada was the Research Chair of the Royal Academy of Engineering in 2013 and also the Chair of the IEEE IES Electrical Machines Committee. He was an Associate Editor of the IEEE TRANSACTIONS ON INDUSTRY APPLICATIONS.